Journal of Catalysis 281 (2011) 40–49

Contents lists available at ScienceDirect

Journal of Catalysis

journal homepage: www.elsevier.com/locate/jcat

Bimetallic Au–Ag/TiO_2 catalyst prepared by deposition–precipitation: High activity and stability in CO oxidation

Alberto Sandoval [a], Antonio Aguilar [a], Catherine Louis [b], Agnès Traverse [c], Rodolfo Zanella [a,*]

[a] Centro de Ciencias Aplicadas y Desarrollo Tecnológico, Universidad Nacional Autónoma de México, Circuito Exterior S/N, Ciudad Universitaria, A.P. 70-186, Delegación Coyoacán, CP 04510, México, DF, Mexico
[b] Laboratoire de Réactivité de Surface, Université Pierre et Marie Curie—UPMC, UMR CNRS 7197, 4, place Jussieu, Case 178, 75252 Paris Cedex 05, France
[c] Laboratoire de Chimie Physique, UMR CNRS 8000, Université Paris Sud, Bât. 349, 91405 Orsay Cedex, France

ARTICLE INFO

Article history:
Received 25 February 2011
Revised 31 March 2011
Accepted 2 April 2011
Available online 17 May 2011

Keywords:
CO oxidation
Bimetallic catalysts
Gold
Silver
Titania
Stability
Deposition–precipitation
Urea
NaOH

ABSTRACT

Au–Ag bimetallic catalysts supported on TiO_2 were prepared by sequential deposition–precipitation method, silver first and then gold. Au–Ag catalysts with different Au/Ag atomic ratios were synthesized. XANES and H_2 TPR results show that gold is more easily reduced in bimetallic catalysts than in Au/TiO_2. The difference in gold reducibility might result from interaction between Au and Ag species. The Au–Ag/TiO_2 catalysts present better temporal stability than monometallic gold catalysts at 20 °C in the reaction of CO oxidation. Compared to monometallic catalysts, the better catalytic results indicate a synergetic effect between gold and silver in the reaction of CO oxidation. The highest catalytic activity was obtained for the catalyst with an Au/Ag ratio of 1:0.37. Temperature of activation under H_2 has also an important consequence on the catalytic activity since conversion increases as temperature increases and reached a maximum for the activation temperature of 550 °C. This optimum results from a compromise between metal particle size, which increases with the activation temperature between 350 and 650 °C, and the bimetallic character of the particles determined by UV–visible and micro-EDS, which improves with the activation temperature. The use of a reducible support such as titania does not lead to much more active catalysts than those supported on nonreducible supports such as silica, probably indicating that the whole reaction takes place mainly on the bimetallic particles.

1. Introduction

Since the discovery in the late eighties that gold is catalytically active when it is dispersed as small particles on an oxide support, the preparation of gold-based catalysts has been widely studied [1–5]. They are active in many reactions of both industrial and environmental importance. The most remarkable catalytic properties of supported gold have been obtained for CO oxidation at ambient temperature [3–6]. The catalytic activity strongly depends on the particle size and is highest in the range of 1–3 nm [7–10]. However, it decreases during the catalytic run. Deactivation has been proposed to be due to nanoparticles sintering [11–14] or to the formation of carbonates adsorbed onto the reactive sites of the catalysts [15,16]. Hence, in spite of their good initial catalytic activity, these catalysts still have very few commercial applications [17].

A way to overcome the deactivation process is to prepare bimetallic catalysts. The physical and chemical properties of bimetallic particles are usually different from those of their single metal counterparts, and they vary significantly as a function of composition and particle size. The enhanced properties of bimetallic metal catalysts are generally attributed to either ensemble or ligand effects, although other factors, related to particle size effects and matrix effects, have been invoked [18].

On the other hand, still in the case of CO oxidation, the Au nanoparticles are known to adsorb CO molecules onto their low-coordination sites. If molecular oxygen is known to interact with Au nanoparticles to some extent, the question of oxygen activation is still a matter of discussion, and oxide supports, such as titania, are known to favor oxygen activation. A way to improve the ability of Au to activate oxygen is to alloy it with a second metal having a stronger affinity for O_2.

Indeed, bimetallic combinations such as Au–Ag exhibit significantly improved activity and stability and synergetic effects, for several reasons. Silver can chemisorb O_2 [19]; silver is also know as a catalyst for CO oxidation, but at higher temperatures than gold [20,21]. Compared with gold, which is the most electronegative metal, Ag has a greater electron-donating ability and could modify the electronic properties of gold. Moreover, the presence of a second metal can induce geometric modifications of the surface of the gold particles.

* Corresponding author. Fax: +52 55 55500654.
E-mail address: rodolfo.zanella@ccadet.unam.mx (R. Zanella).

0021-9517/$ - see front matter © 2011 Elsevier Inc. All rights reserved.
doi:10.1016/j.jcat.2011.04.003

Some studies have indeed shown the potentiality of Au–Ag catalysts for CO oxidation. For instance, Iizuka et al. [22,23] found that silver impurities in unsupported gold nanoparticles enhance their catalytic activity in CO oxidation. Wang et al. [24–26] reported that Au–Ag alloy catalyst supported on mesoporous aluminosilicate was active and stable for low-temperature CO oxidation.

Gold and silver are miscible in all proportions, due to very close lattice constants [27–29], so the Au/Ag ratio can be varied within a wide range. Only a few methods have been used to prepare supported Au–Ag catalysts. Two of them were developed by Wang et al.: a one-pot method involving preformed Au–Ag colloids in a hydrothermal treatment to synthesize MCM-41 mesoporous supports [25,26], yielding metal particles larger than 15 nm, and a two-pot method involving successive ion adsorption of gold and then silver on MCM-41 [30] and on commercial silica and alumina [31], leading to smaller bimetallic particles (3–4 nm). A third method consists in the co-impregnation of SiO_2–Al_2O_3 with gold and silver precursors followed by bioreduction, which leads to bimetallic particles of 5 nm [32].

The goal of this work was to prepare Au–Ag catalysts on a reducible TiO_2 support by a new method based on deposition–precipitation and to obtain small metal particles. Deposition–precipitation with urea and with NaOH has been used extensively to prepare monometallic gold catalysts supported on oxide supports [3,33,34] and bimetallic catalysts such as Au–Ir [35,36] and Au–Pd [37] catalysts. To the best of our knowledge, this method has never been used to prepare Au–Ag bimetallic catalysts, and Au–Ag catalysts supported on titania have never been tested in CO oxidation. Such Au–Ag samples have been prepared by this method, characterized, and tested in CO oxidation. Preliminary results have shown that better catalysts in terms of catalytic performance were obtained by sequential deposition–precipitation, silver first and then gold rather than gold first and then silver, or by co-deposition–precipitation. So, this method is presented in this paper.

2. Experimental

2.1. Catalyst preparation

2.1.1. Preparation of monometallic samples

Titania Degussa P25 was used as support (45 $m^2\,g^{-1}$, nonporous, 70% anatase and 30% rutile, purity >99.5%). Commercial $HAuCl_4{\cdot}3H_2O$ and $AgNO_3$, both from Aldrich, were used as gold and silver precursors. Before preparation, TiO_2 was dried in air at 100 °C for at least 24 h. The nominal metal loadings in the monometallic catalysts were 4 wt.% for Au and 2.2 wt.% for Ag, which corresponds to 0.56 at.% for both samples.

The preparation of a Au/TiO_2 sample with 4 wt.% Au as theoretical loading was performed by deposition–precipitation with urea (DPU) in the absence of light following the previously reported procedure [33,38,39]. Briefly, the gold precursor, $HAuCl_4$ (4.2×10^{-3} M), and the urea (0.42 M) were dissolved in 50 ml of distilled water; the initial pH of the solution was 2.4. Then, 1 g of titania was added to this solution; thereafter, the suspension temperature was increased to 80 °C and kept constant for 16 h under stirring.

The preparation of Ag/TiO_2 with 2.2 wt.% Ag as theoretical loading was performed by deposition–precipitation with NaOH (DPNaOH). For some reasons, not yet elucidated, Ag could not be deposited on the support by DPU. Ag/TiO_2 was prepared as follows: 1 g of TiO_2 was added to 54 ml of an aqueous solution containing $AgNO_3$ (4.2×10^{-3} M). The solution was heated to 80 °C. The initial pH was ~3; then, the pH was adjusted to 9 by dropwise addition of NaOH (0.5 M), promoting AgOH precipitation on TiO_2. The suspension was vigorously stirred for 2 h at 80 °C.

After the deposition–precipitation procedure, all samples were centrifuged, washed with water four times, centrifuged again, and dried under vacuum for 2 h at 80 °C. After drying, the samples were stored at room temperature in a desiccator under vacuum, away from light, in order to prevent any alteration [39].

2.1.2. Preparation of bimetallic samples

The gold amount in the solutions corresponded to a nominal loading of 4 wt.% on the support, while that of silver was chosen to synthesize Au–Ag catalysts with different nominal Au/Ag atomic ratios: 1:0.25, 1:0.5, 1:0.75, 1:1, and 1:1.5, i.e., 0.6, 1.2, 1.7, 2.2, and 3.3 wt.% Ag. A sequential deposition method was used to prepare the bimetallic catalysts. Silver was first deposited on TiO_2 according to the DPNaOH method described above; only the silver concentration was changed to get the chosen nominal Ag loading. After drying at 80 °C for 2 h, gold was deposited by the DPU method. Then, these samples were washed, dried, and stored as described above. The samples are identified as Au–Ag followed by the Au/Ag atomic ratio, e.g., Au–Ag 1:0.5.

2.2. Catalytic activity

The CO oxidation reaction was studied in a flow reactor at atmospheric pressure and increasing temperature range from −5 to 500 °C (light-off test). A sample of 0.04 g of dried catalyst was first activated in situ in a flow of 40 ml/min of hydrogen with a heating rate of 2 °C/min up to the final activation temperatures, followed by a temperature plateau of 2 h. After this treatment, the sample was cooled to −5 °C under the same gas. The reactant gas mixture (1 vol.% CO and 1 vol.% O_2, balance N_2) was introduced with a total flow rate of 100 ml/min, and the heating rate was 2 °C/min. The gases were analyzed with an Agilent Technologies 6890 N online gas chromatograph equipped with a FID detector and an HP Plot Q column.

Stability of the catalysts vs. time on stream was examined at 20 °C during a 24-h run after activation in situ, using 30 mg of catalyst activated in situ in hydrogen at the same heating rate and temperature plateau as described above.

2.3. Characterization techniques

Chemical analysis of Au and Ag in the dried samples was performed by ICP in a Perkin Elmer Optima 4300 DV optical emission spectrometer. The Au and Ag weight loadings were expressed in grams of each metal per gram of sample.

Thermal treatments for UV–visible and electron microscopy characterization were performed under the same conditions as for CO oxidation reaction: in a U reactor with a fritted plate of diameter 1.5 cm under a flow of H_2 (1ml min^{-1} mg^{-1}_{sample}) with a heating rate of 2 °C/min up to a final temperature between 200 and 650 °C and a temperature plateau of 2 h.

Diffuse reflectance UV–visible spectra of the catalysts were obtained using an Ocean Optics USB2000 miniature fiber optic spectrometer (ex situ reduction, according to the conditions given).

X-ray absorption near-edge structure (XANES) measurements on Au/TiO_2, Ag/TiO_2, and Au–Ag/TiO_2 were performed at the Au L_{III}-edge and at the Ag *K*-edge at the SAMBA beam line of the SOLEIL synchrotron radiation facility (France) using a channel-cut Si [111] monochromator. The catalysts were measured in the fluorescence mode, with 0.5-eV steps from 11,700 to 12,020 eV for the Au L_{III}-edge and from 25,400 to 25,600 for the Ag *K*-edge. The samples were placed in the sample holder of a Harrick Scientific Products high-temperature cell for in situ experiments [40]. Each dried sample was first measured in the initial state (dried) under helium flow (50 ml/min) at room temperature (RT), then helium flow was replaced by pure hydrogen flow (50 ml/min), and the sample was

heated at a rate close to 2 °C/min, i.e., under the same conditions as those of activation before the catalytic reaction up to complete reduction. The XANES scan time was 7 min at the Au edge and 17 min at the Ag edge. The Au–Ag/TiO_2 sample was studied twice, each time with a new dried sample, at both the Au and Ag edges. Reference samples were measured in air at RT in transmission mode using two argon-filled ionization chambers. Energy calibration of the monochromator was done using Au and Ag foil. For Ag^0 and for Au^0, silver foil and gold foil with thickness adjusted to get a jump of about 1 at the edge were measured. Pellets of Ag_2O for Ag^+, of AgO for Ag^{2+}, and of Au_2O_3 for Au^{3+} were prepared from the respective powders mixed with cellulose in proportions calculated to get a jump of about 1 at the edge. After background subtraction, the XANES spectra were normalized at E = 11,981 for Au and E = 25,536 for Ag. To follow the evolution of the gold oxidation state of the samples at the Au L_{III}-edge, the intensity of the white line was extracted by subtraction of a baseline fitted with a sigmoid function passing through 11, 900–11,917 and 11,928–11,930 eV, followed by the integration of the white line.

Hydrogen temperature-programmed reduction (H_2 TPR) of the dried catalysts was performed in a RIG-150 unit under a flow of 10% H_2/Ar gas mixture (30 ml min^{-1}) and a heating rate of 10 °C/min from room temperature to 300 °C. H_2O produced during the reduction process was trapped before the TCD detector.

After ex situ reduction (2 °C/min under 40 ml/min of hydrogen up to a chosen temperature, and then a plateau for 2 h), the samples were examined by transmission electron microscopy in a Jeol-2010 FasTem analytical microscope equipped with a Z-contrast annular detector and an EDS detector. The average size of gold particles and the histograms of particle sizes were established from the measurement of 800–1000 particles. The size limit for the detection of gold particles on TiO_2 was about 0.6 nm. The average particle diameter d_s was calculated using the formula $d_s = \sum n_i d_i / \sum n_i$, where n_i is the number of particles of diameter d_i. The standard deviation was calculated with the formula $\sigma = [\sum (d_i - d_s)^2 / \sum n_i]^{1/2}$. The micro-EDS measurements were performed on an Au–Ag catalyst activated at different temperatures under the same conditions as for the CO oxidation reaction. In every case, about 40 individual particles randomly selected in a unique zone of the catalyst were analyzed.

3. Results

3.1. Elemental analysis

Let us recall that the nominal metal loadings of the monometallic catalysts were 4 wt.% for Au and 2.2 wt.% for Ag, which corresponds to 0.56 at.% for both samples. Table 1 compares the nominal and the measured gold and silver loadings in wt.% and the Au/Ag atomic ratios for the Au–Ag samples. As expected for Au/TiO_2, practically all the gold present in solution was deposited on TiO_2. In the case of Ag/TiO_2, about 90% of the silver present in solution was deposited on TiO_2. In the case of bimetallic samples, the actual gold loadings are also very close to the theoretical value (4 wt.%), whereas for silver, the actual loading is always lower than the nominal loading. Since silver was first deposited on TiO_2, leaching of silver may have occurred during Au deposition. In the following, the Au–Ag samples are designated by their actual loadings.

3.2. Influence of the Au/Ag atomic ratio and the pretreatment temperature on CO oxidation activity and temporal stability

Fig. 1a shows the conversion of CO as a function of the reaction temperature for Au–Ag/TiO_2 catalysts prepared with different Au/Ag atomic ratios after activation under H_2 at 550 °C. The catalytic activity of the monometallic catalysts is also reported for comparison. The Au/TiO_2 sample is already active at −5 °C (CO conversion ≈49%). whereas at temperatures lower than 60 °C, Ag/TiO_2 is completely inactive. The Au–Ag samples with atomic ratios 1:0.15, 1:0.37, 1:0.66, 1:0.76, and 1:0.9 show a higher conversion than Au/TiO_2.

The Au–Ag 1:0.76 catalyst was used to perform a systematic study of the influence of the temperature of activation in H_2. Fig. 1b shows that the sample pretreated at 550 °C is the most active. Activation temperatures lower than 350 °C (300 and 200 °C) were also tested, but the catalyst presented catalytic activity lower than that of the sample treated at 350 °C. The dried sample did not show any activity at room temperature, and the CO conversion remained lower than 10% at 200 °C. Note that the activation of Au–Ag samples under air systematically produced lower catalytic activity.

To determine the stability of the Au–Ag catalysts, time-on-stream experiments were performed at 20 °C for 24 h. Fig. 2 shows the results of Au/TiO_2, Au–Ag 1:0.66, and Au–Ag 1:0.15 catalysts activated in H_2 at 550 °C. While Au/TiO_2 deactivates continuously during the 24 h on stream, the bimetallic Au–Ag 1:0.66 catalyst becomes stable after 2–3 h, during which time it activates. The catalyst with the lower Ag loading (Au–Ag 1:0.15) is less stable than Au–Ag 1:0.66. It is important to note that the CO conversion was at maximum 65%. Under the same conditions, CO conversion over Au–Ag 1:0.76 and Au–Ag 1:0.37 was 100%. Hence, the addition of even a small proportion of Ag leads to much more stable catalysts than monometallic gold.

To attempt to explain the catalytic results, characterizations were performed either on the series of bimetallic samples after activation at 550 °C, or for the Au–Ag 1:0.76 samples at different activation temperatures. Comparisons are made with monometallic samples.

3.3. XANES characterization

Fig. 3a and b present the normalized XANES spectra of Au/TiO_2 and Au–Ag/TiO_2 1:0.76 as a function of the activation temperature under H_2 compared with Au_2O_3 and Au as reference. As the spectra were recorded during heating, the temperatures reported on the

Table 1
Theoretical and actual Au and Ag loadings in the studied catalysts.

Nominal composition	Metal loading (wt.%)				Actual Au/Ag atomic ratio
	Nominal Au loading	Actual Au loading	Nominal Ag loading	Actual Ag loading	
Au	4	3.8	0	0	–
Ag	0	0	2.2	2.0	–
Au–Ag 1:0.25	4	3.8	0.6	0.3	Au–Ag 1:0.15
Au–Ag 1:0.5	4	3.9	1.2	0.8	Au–Ag 1:0.37
Au–Ag 1:0.75	4	3.8	1.7	1.4	Au–Ag 1:0.66
Au–Ag 1:1	4	3.9	2.2	1.6	Au–Ag 1:0.76
Au–Ag 1:1.5	4	3.9	3.3	1.9	Au–Ag 1:0.90

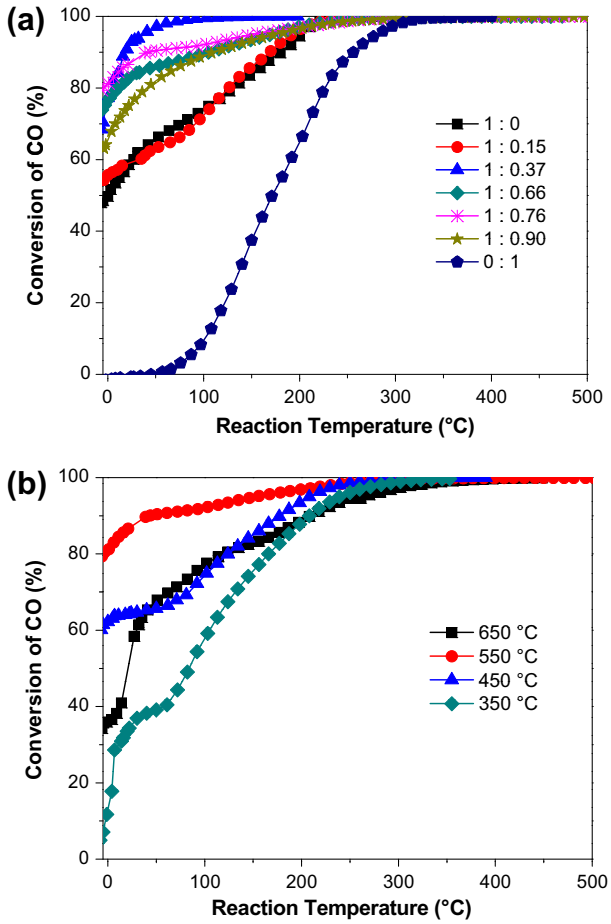

Fig. 1. CO oxidation light-off curves of (a) monometallic Au and Ag and bimetallic Au–Ag catalysts activated at 550 °C under H_2; (b) catalyst Au–Ag 1:0.76 as a function of the temperature of pretreatment in H_2.

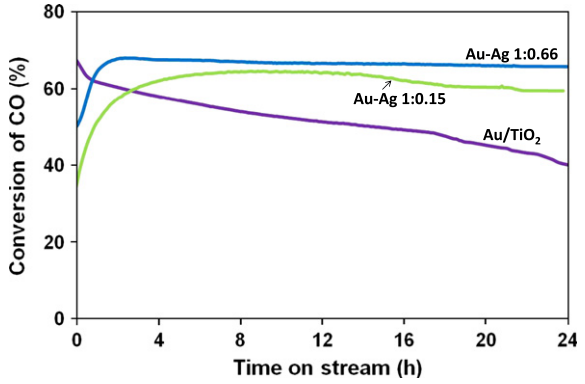

Fig. 2. Evolution of conversion of CO (%) as a function of time on stream at 20 °C for the Au/TiO_2, Au–Ag 1:0.15, and Au–Ag 1:0.66 catalysts reduced in H_2 at 550 °C.

figures are those that correspond to the middle of the spectra. The Au^{III} spectrum of the Au_2O_3 reference differs from the Au^0 spectrum of the Au reference in the intensity of the white line at ≈11,922 eV. For both catalysts, the Au edge is initially similar to that of Au^{III}, indicating that gold is still mainly present in the oxidized form after drying. Then, it reduces to Au^0 when temperature increases, mainly between 50–80 and 120 °C. At 160 °C, the XANES spectrum of Au/TiO_2 is very similar to that of metallic gold. In Au–Ag 1:0.76, reduction begins at a lower temperature (≈40 °C) and is also over at a lower temperature (≈100 °C) (Fig. 3b). The variation

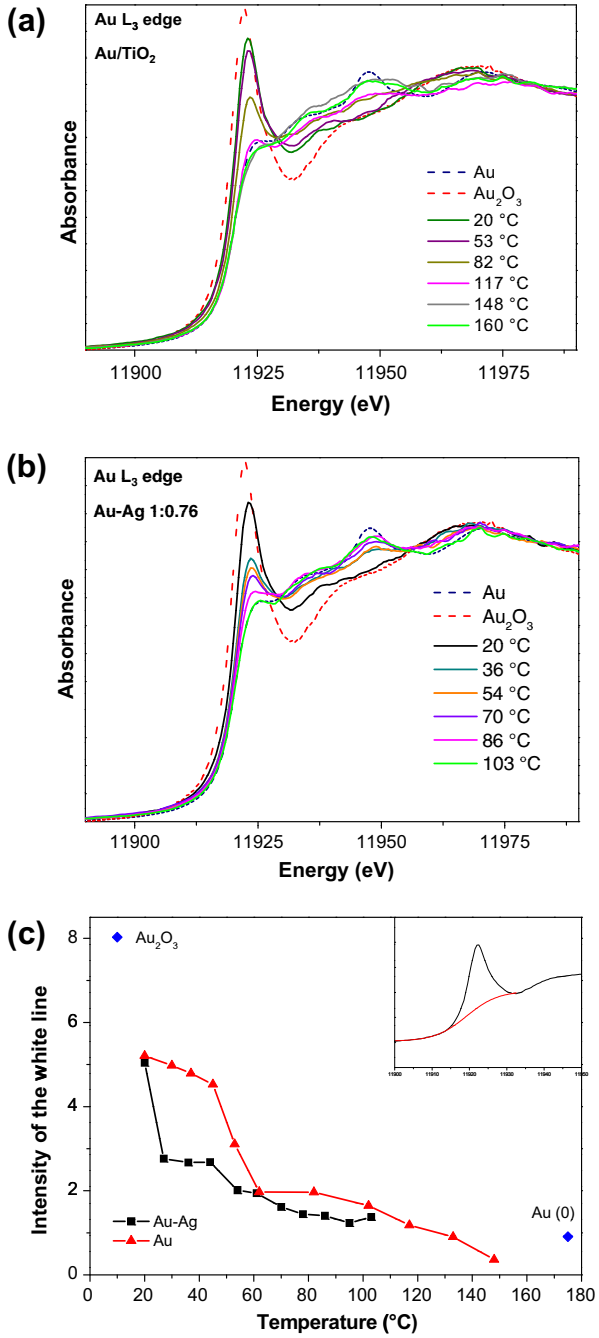

Fig. 3. XANES spectra at the Au L_{III}-edge of (a) Au/TiO_2 catalyst after drying at 80 °C and during activation in hydrogen at increasing temperatures and Au^0 and Au^{III} (Au_2O_3) references; (b) Au–Ag 1:0.76 catalyst after drying at 80 °C and during activation in hydrogen at increasing temperatures. (c) Intensity of the white lines of Au/TiO_2 and Au–Ag 1:0.76 at the Au L_{III}-edge versus activation temperature.

of the white line intensity with temperature plotted in Fig. 3c confirms that gold in Au–Ag 1:0.76 catalyst is more easily reduced than that in Au/TiO_2. The shape of the two graphs is discussed later.

Fig. 4a and b show the XANES spectra at the Ag *K*-edges of Ag/TiO_2 and Au–Ag 1:0.76 samples in the initial state after drying and after thermal treatments; they are compared with the Ag^0 and Ag^I (Ag_2O) references. The main difference is seen in the initial state: Ag in Ag/TiO_2 is already in the metallic state after drying, whereas the edge of Ag in $Au–Ag/TiO_2$ does not correspond to that of Ag^0, nor to that of Ag_2O. Increasing temperature under H_2 induces the reduction in Ag in Au–Ag between 60 and 150 °C.

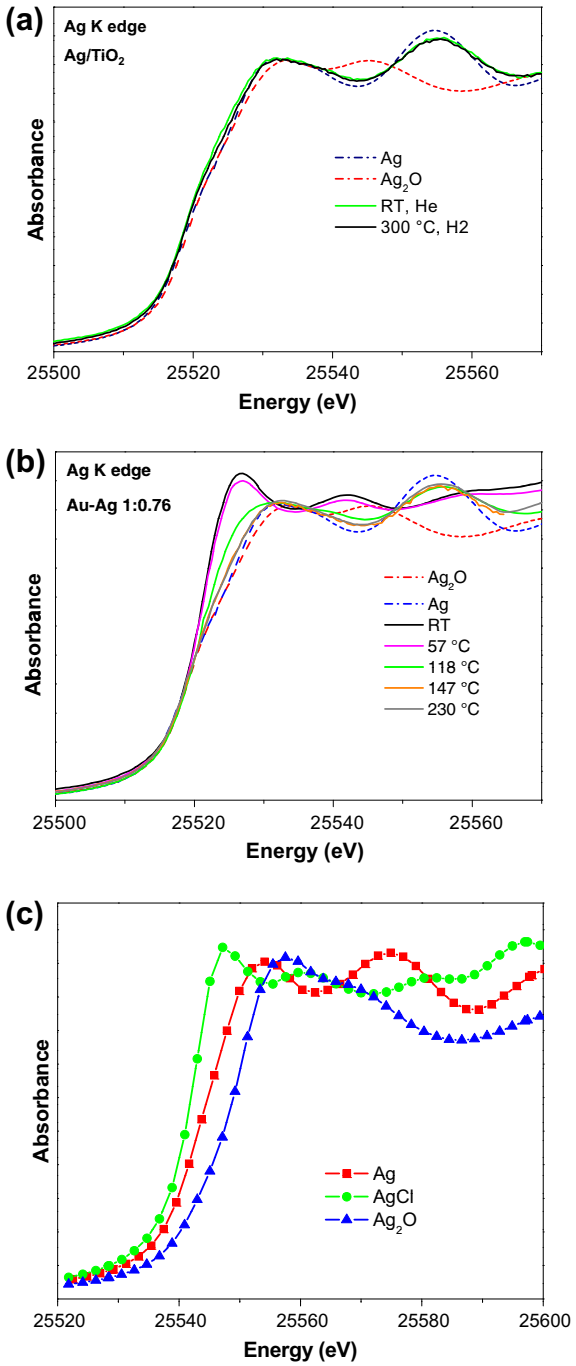

Fig. 4. XANES spectra at the Ag K-edge of (a) Ag/TiO_2 catalyst after drying at 80 °C and after activation in hydrogen at 300 °C and Ag^0 and Ag^I (Ag_2O) references; (b) Au–Ag 1:0.76 catalyst, after drying at 80 °C and during activation in hydrogen at increasing temperatures. (c) FEFF8 simulations of the XANES spectra at the Ag *K*-edge of Ag_2O, Ag^0, and AgCl.

To interpret the XANES spectra at the Ag *K*-edge of the bimetallic sample before thermal treatment, the XANES spectra of Ag_2O, Ag, and AgCl were calculated using the FEFF 8.0 code [41] (Fig. 4c). For Ag_2O and Ag, although the edge position is shifted, due to the difficulty of calculating the self-energy [42], the XANES shapes are similar to the experimental ones (Fig. 4a and b), which validates the comparison between calculated and experimental spectra. So the fact that the calculated XANES of AgCl has a shape similar to the experimental signal after drying is an indication that the initially deposited Ag species have reacted, at least partially, with chlorides introduced during DPU of Au ($HAuCl_4$ precursor). The easy formation of AgCl by reaction of Ag^+ species and Cl^- is frequently evoked in the literature related to the synthesis of supported Au–Ag particles [31,32]. However, the formation of AgCl requires that Ag in the metallic state on titania before gold deposition be reoxidized. Consider the following redox potentials [43]:

$$AgOH \text{ or } Ag_2O + H_2O + 2e^- \rightleftarrows 2Ag + 2OH^- + 0.342 - 0.345 \text{ eV}$$
$$AuCl_4 + 3e^- \rightleftarrows Au + 4Cl^- + 0.994 - 1.002 \text{ eV}.$$

The Au^{3+}/Au redox potential is higher than that of Ag^+/Ag; as a consequence, the gold precursor is indeed able to oxidize metallic silver.

3.4. TPR characterization

The reducibility of the catalysts was also studied by TPR. Fig. 5 displays the TPR profiles of Au/TiO_2, Ag/TiO_2, and the bimetallic $Au–Ag/TiO_2$ samples. In the case of Ag/TiO_2, no reduction peak is observed, which confirms the XANES result (Fig. 4a) that Ag was already reduced in the dried sample. In the case of Au/TiO_2, the reduction profile is characterized by a peak with a maximum at T = 120 °C. The reduction in the sample begins at 100 °C and ends at ≈165 °C, in agreement with the XANES results, which showed that Au was still in the oxidized form after drying, and was reduced between 50–80 and 160 °C.

For the bimetallic samples, the reduction profile is characterized by a peak with a maximum at temperatures between 122 and 126 °C, i.e., close to that of Au/TiO_2. However, some differences are observed if one considers the temperatures at which reduction starts and ends. In $Au–Ag/TiO_2$ samples, reduction starts and ends at lower temperatures ($T_{start} \approx 75$ °C, $T_{end} \approx 150$ °C, respectively) than in Au/TiO_2 (T_{start} = 100 °C, T_{end} = 160 °C), which is consistent with the XANES results: reduction between 50 and 100 °C for gold and between 60 and 150 °C for silver (Figs. 3 and 4).

3.5. UV–visible characterization

The UV–visible spectra (Fig. 6a) of the monometallic and bimetallic catalysts reduced at 550 °C show a broad absorption band due to the surface plasmon resonance (SPR) of gold and silver. The plasmon band is centered at 560 nm for Au/TiO_2 and 480 nm for Ag/TiO_2, and the absorption band is blue-shifted from 560 to 540 nm as the percentage of silver increases in the bimetallic catalysts; the width of the surface plasmon band increases as well.

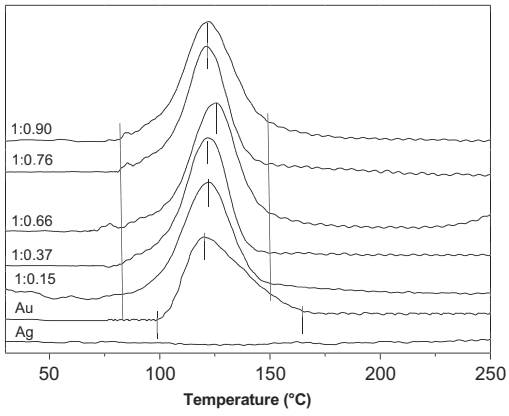

Fig. 5. TPR profiles of monometallic Au/TiO_2 and Ag/TiO_2 and bimetallic Au–Ag catalysts with various Au/Ag ratios.

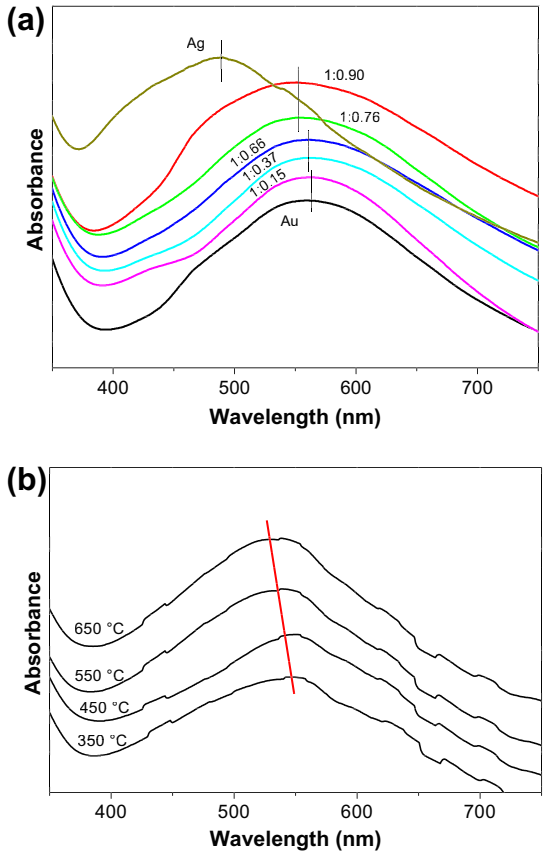

Fig. 6. UV–visible spectra of (a) Au/TiO_2 and Ag/TiO_2 and bimetallic Au–Ag catalysts with various Au/Ag ratios after activation in H_2 at 550 °C; (b) catalyst Au–Ag 1:0.76 after different temperatures of activation in H_2.

Fig. 6b shows the UV–visible spectra of the Au–Ag 1:0.76 sample activated at various temperatures between 350 and 650 °C. The maximum of the absorption band shifts from 554 to 540 nm as the temperature increases, while the bandwidth becomes slightly narrower.

3.6. Electron microscopy: size and composition of the nanoparticles

Fig. 7 shows typical images of Au–Ag 1:0.76 reduced in hydrogen at 350, 450, 550, and 650 °C. The average metal particle size and the size distribution, reported in Table 2 and Fig. 8, increase with temperature. Table 3 reports the metal particle size in the Au–Ag catalysts with different Ag/Au ratios and after activation at 550 °C. Whatever the Au/Ag ratio, the average particle size is the same, 3.7–3.9 nm. The particles are much smaller than the Ag particles in Ag/TiO_2 (9 nm) and almost the same size as gold particles in Au/TiO_2 (4.1 nm).

To determine the homogeneity of the composition of the particles in bimetallic samples, a systematic study of the Au–Ag 1:0.76 catalyst reduced in H_2 at 350, 550, and 650 °C was performed by micro-EDS coupled to transmission electron microscopy. For each sample, about 40 individual particles randomly selected in a unique zone of the catalyst were analyzed. Table 2 reports the percentage of mixed particles (particles that contain both Au and Ag) and also the percentage of particles that have an Au/Ag atomic ratio close to the actual Au/Ag ratio, i.e., 1:0.76.

When the sample is treated at 350 °C, three kinds of particles are observed: monometallic Au and Ag (in low proportion) and bimetallic Au–Ag (75%). Among the 75% of bimetallic particles, only 10% have an Au/Ag atomic ratio close to the actual Au/Ag ratio. The particle composition in this sample is therefore not homogeneous. When the sample is treated at 550 °C, 90% of the particles are bimetallic and about 30% of them have an Au/Ag ratio close to the actual Au/Ag ratio determined by chemical analysis. In the sample treated at 650 °C, all of the particles analyzed are bimetallic and about 60% of them have an Au/Ag ratio close to the actual ratio.

4. Discussion

4.1. Oxidation state of gold and silver in the dried samples

According to XANES (Fig. 3a) and TPR (Fig. 5), gold in dried Au/TiO_2 is mainly present in the oxidized state III, in agreement with former work [10,38]; this is also true for gold in $Au–Ag/TiO_2$ (Fig. 3b). In contrast, Ag in dried Ag/TiO_2 is already reduced after drying (XANES in Fig. 4a and TPR in Fig. 5), whereas in $Au–Ag/TiO_2$, it is still in the oxidized state I and in the form of AgCl, as already discussed (Fig. 4b). The reason for the different oxidation states of silver may be that AgCl in $Au–Ag/TiO_2$ is less reducible than AgOH in Ag/TiO_2, or that interaction with the gold precursor, i.e., the gold–urea complexes formed during DPU [38], inhibits silver reduction. On the other hand, it is possible that the silver fraction, which is leached during the washing step after Au DPU, and leads to lower Ag loading in $Au–Ag/TiO_2$ than in Ag/TiO_2 (Table 1), is some of the precipitated AgCl not interacting with the support.

4.2. Reducibility of gold and silver

Gold reduction occurs at a lower temperature in $Au–Ag/TiO_2$ 1:0.76 (total reduction at 100 °C according to XANES in Fig. 3b) than in Au/TiO_2 (total reduction at 160–165 °C according to XANES (Fig. 3a) and to TPR (Fig. 5)). Such low-temperature reduction has already been observed in Au/TiO_2 samples [44–46]. According to Fig. 3c, the reduction in gold occurs in two steps, first fast reduction in most of the gold and then slow reduction in the remaining gold; this reduction process is shifted toward lower temperature in the case of $Au–Ag/TiO_2$. The difference in gold reducibility might result from interaction between Au and Ag species.

In contrast, reducibility of silver is delayed in $Au–Ag/TiO_2$ 1:0.76 (total reduction at 150 °C according to XANES, Fig. 4b) compared with Ag/TiO_2, in which Ag is already reduced after drying at 80 °C. As mentioned earlier, the reason could be that the silver precursors are different in the two samples, AgCl and AgOH. As the reduction in gold occurs at lower temperature than that of silver, according to XANES, the TPR profile of Au/Ag catalysts can be interpreted as a combination of the reduction in both metal precursors, gold first, at the beginning of the reduction peak, and then silver, in the latter part of the reduction peak.

4.3. Evolution of the metal particles in the reduced samples

Once reduction in gold and silver is over above 150 °C, and when higher hydrogen thermal treatments are applied, between 350 and 650 °C, the average size of the metal particles increases. Meanwhile, the metal particles become more bimetallic (Table 2). After activation at 350 °C, micro-EDS shows that only 75% of the particles are bimetallic. This is probably because the two metals were sequentially deposited on the support (first silver, then gold) and do not interact with each other until both gold and silver or gold or silver atoms become mobile when the activation temperature is high enough. Since gold and silver are miscible in all proportions, mobility favors the formation of bimetallic particles. The fact that metal particle size increases and the

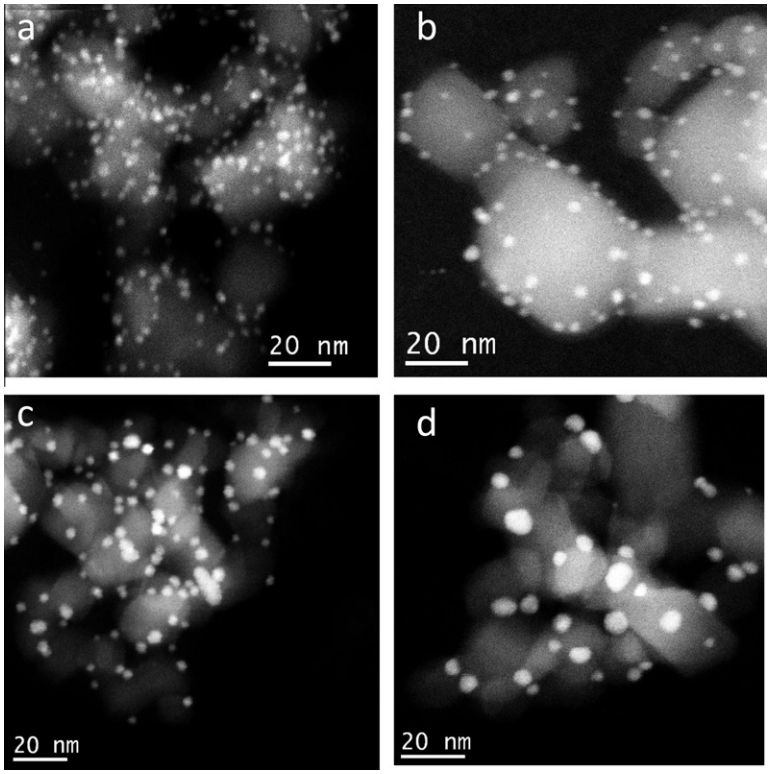

Fig. 7. HAADF images of Au–Ag 1:0.76 catalyst after different temperatures of activation in H_2: (a) 350 °C, (b) 450 °C, (c) 550 °C, (d) 650 °C.

Table 2
Evolution of the average particle size and particle composition (determined by micro-EDS) in catalyst Au–Ag 1:0.76 as a function of the activation temperature.

Activation temperature (°C)	Average particle size (nm)	Standard deviation (nm)	% of particles containing both Au and Ag	% of particles with Au/Ag ratio of 0.76 ± 0.08
350	2.6	0.63	75	10
450	3.3	0.72	–	–
550	3.9	0.99	90	30
650	5.4	1.80	100	60

particles become more bimetallic as the activation temperature increases from 350 to 650 °C (Table 2) is in line with this interpretation. In a former study [47], some of us showed that the size of gold particles in Au/TiO_2 prepared by DPU barely changed during reduction under H_2 between 300 and 500 °C, from 1.7 to 2.1 nm. We can therefore tentatively propose that the increase in size observed in the Au–Ag samples results from silver mobility and leads to larger particles, but also to particles more homogeneous in composition, as observed by micro-EDS (Table 2).

The UV–visible spectra of $Au–Ag/TiO_2$ 1:0.76 (Fig. 6b) slightly change with the activation temperature; the maximum of the absorption band shifts from 555 to 540 nm, and the bandwidth becomes slightly narrower as activation temperature increases. This could be also an indication of the formation of more homogeneous particles. However, this could be also due to enrichment of the particles' surface with silver when the activation temperature is increased. Indeed, Wang et al. [24] in a study with Au–Ag/MCM41 catalysts proposed, based on complementary XPS experiments, that the blue shift of the SPR band with the higher reduction temperature implied changes in particle surface composition and surface enrichment with Ag. The change in the position of the maximum SPR could also be related to change of metal particle size [48], which also occur when the temperature of activation is increased (Table 2).

4.4. Catalytic properties of Au–Ag catalysts pretreated at various temperatures

Activation temperature has an important consequence for catalytic performance, because conversion increases when activation temperature increases (Fig. 1b), but it reaches a maximum at an activation temperature of 550 °C. This optimum may result from the fact that as the activation temperature increases, on the one hand, the particle becomes more bimetallic and more homogeneous in composition, according to micro-EDS (Table 2), which is advantageous for activity (synergetic effect), but on the other hand, the particles increase in size (Table 2), which is detrimental for activity. The highest activity at 550 °C may therefore result from a compromise between particle size and particle composition.

Wang et al. [26] previously reported that reduction in Au–Ag/MCM-41 at 550–600 °C also led to the highest activity in CO oxidation at room temperature. They also provided evidence for a synergetic effect between gold and silver in Au–Ag catalysts on various nonreducible supports such as MCM-41, SiO_2, and Al_2O_3 [24–26,30,31]. They proposed that Ag plays a key role in the activation of oxygen and that particle size is not a critical factor, as in the case of monometallic gold catalysts. In a detailed study on the adsorption of oxygen on Au–Ag alloy particles of about 100 nm supported on alumina, Kondarides and Verykios [49] found that molecular oxygen adsorption on Ag is favored by the presence of Au. Wang et al. [26] proposed that oxygen could be adsorbed and activated on the Ag sites of the alloy particle surface, while CO adsorbs on Au. Note that it has been shown previously that CO adsorption on gold occurs only on low-coordinated sites [10,50]. Wang et al. [26] also proposed that molecular oxygen would be more easily

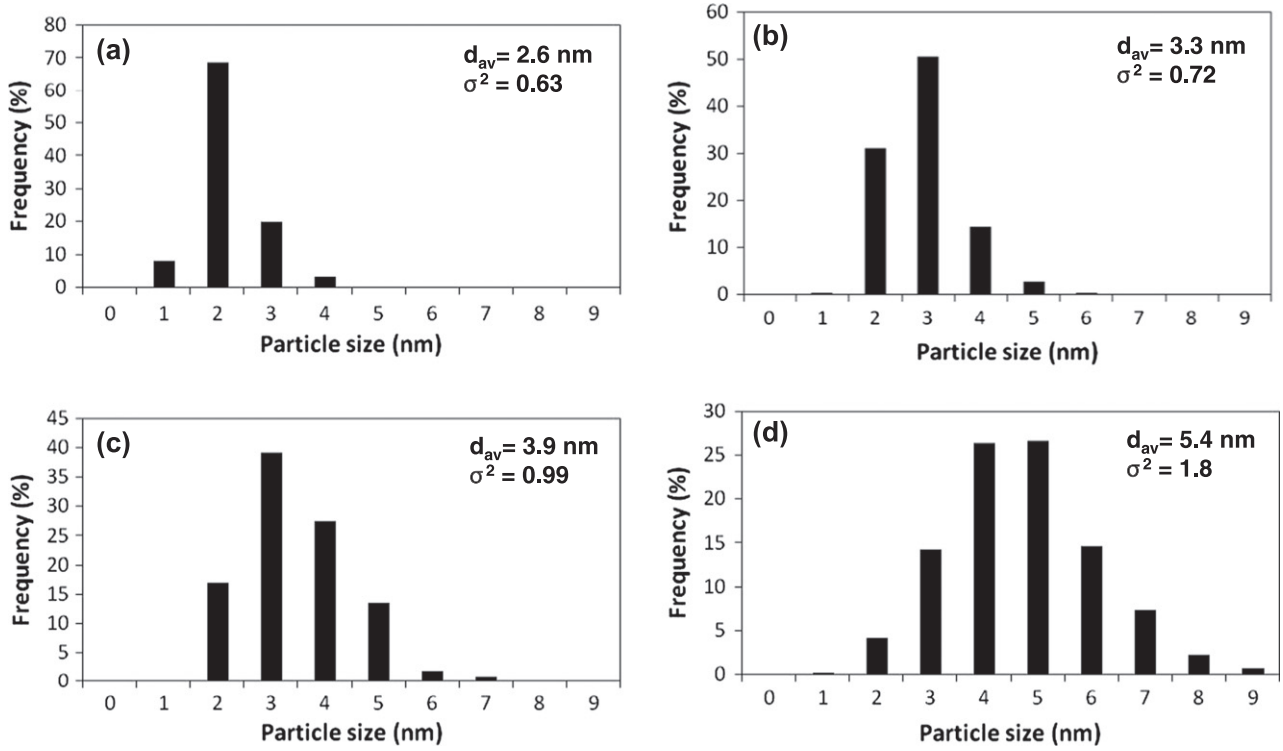

Fig. 8. Histograms of metal particle size in Au–Ag 1:0.76 catalysts after different temperatures of activation in H_2: (a) 350 °C, (b) 450 °C, (c) 550 °C, (d) 650 °C. The average particle size (d_{av}) and the standard deviation (σ^2) are reported.

Table 3
Average particle size in catalysts with various Au/Ag atomic ratios, activated in hydrogen at 550 °C.

Catalyst	Average particle size (nm)	Standard deviation (nm)
Au/TiO_2	4.1	0.82
Au–Ag 1:0.37	3.8	0.86
Au–Ag 1:0.66	3.7	0.82
Au–Ag 1:0.76	3.9	0.99
Au–Ag 1:0.90	3.8	0.87
Ag/TiO_2	9.0	3.40

activated by the Au–Ag ensemble on the surface to form O_2^- species than on Ag. Moreover, their DFT calculation showed that in CO oxidation, an electron transfer from Ag to the antibonding orbital of the O_2 molecule weakens the O–O bonding, thus improving the oxygen activation. With a neighboring adsorbed CO, the oxygen transfer reaction then would occur easily, explaining the synergetic effect between gold and silver.

4.5. Evolution of the catalytic properties with the Au/Ag ratio after activation at 550°C

Whatever the Au/Ag ratio, the average size of the metal particles in the $Au–Ag/TiO_2$ catalyst is constant (3.7–3.9 nm) and is almost the same as that of the monometallic gold particles (4.1 nm), but is much smaller than that of the silver particles in Ag/TiO_2 (9 nm) (Table 3). This suggests that the average particle size in bimetallic catalysts is driven by the presence of gold, which also attests to the existence of Au–Ag interactions.

The UV–visible spectra of the $Au–Ag/TiO_2$ samples activated at 550 °C (Fig. 6a) show that the SPR band is blue-shifted and the bandwidth increases, as the proportion of silver in the bimetallic catalysts increases. In the case of the Au–Ag 1:0.9 sample, a shoulder at 480 nm is clearly visible and can be attributed to the presence of monometallic or poorly bimetallic silver particles. Since we know from micro-EDS (Table 2) that Au–Ag 1:0.76 contains a rather low proportion of bimetallic particles, with an Au/Ag ratio close to the one given by chemical analysis, it can be assumed that in Au–Ag 1:0.9, this proportion is still lower and the proportion of monometallic Ag particles still higher. So the blue shift and the bandwidth increase could result from an increasing proportion of monometallic silver particles, i.e., from an increase in the inhomogeneity of the Au/Ag composition in the particles as the proportion of silver increases.

4.6. Evolution of the catalytic properties with the Au/Ag ratio for catalysts activated at 550°C

It is interesting to note that in the range of temperatures at which Ag/TiO_2 is completely inactive (<60 °C), the Au–Ag samples are more active than gold (Fig. 1a), except Au–Ag 1:0.15, which is not very different from monometallic gold. This is clear evidence of a synergetic effect between gold and silver. Although the samples containing more silver show rather close conversion, it seems that the most active catalyst is Au–Ag 1:0.37 catalyst (Fig. 1a). This result is in agreement with the results by Wang et al. [26], who showed that for a series of Au–Ag catalysts on MCM-41 prepared with preformed colloids, Au–Ag 3:1 catalyst (equivalent to 1:0.33) gave the highest activity in CO oxidation reaction. However, these results are different from those obtained by Wang et al. [51] in another study of CO oxidation over a series of $Au–Ag/SiO_2$ catalysts, also prepared by a colloidal method, which showed that the Au–Ag 1:1 catalyst was the most active catalyst.

In addition to the synergetic effect due to the addition of silver to gold and the formation of bimetallic particles, the $Au–Ag/TiO_2$

Table 4
Comparison of the reaction rates for the CO oxidation of Au–Ag/TiO_2 catalysts with those reported in the literature.

Catalyst	T (°C)	Average particle size (nm)	Contact time ($g_{cat}hmol^{-1}_{CO}$)	Reaction rate ($molmol^{-1}_{Au}s^{-1}$)	Source
Au–Ag 1:0.15	30	–	16	0.070	This work
Au–Ag 1:0.37	30	3.8	16	0.086	This work
Au–Ag 1:0.66	30	3.7	16	0.076	This work
Au–Ag 1:0.76	30	3.9	16	0.079	This work
Au–Ag 1:0.90	30	3.8	16	0.069	This work
Au–Ag/MCM-41 1:0.13	30	4.1	23.4	0.060	[31]
Au–Ag/SiO_2 1:0.31	20	3.3	2.2	0.050	[30]
Au–Ag/SiO_2 1:0.52	20	3.4	2.2	0.028	[30]

catalysts exhibit much better stability than the monometallic gold catalysts in CO oxidation (Fig. 2). The same observation was made by Wang et al. in the case of Au–Ag/MCM41 [25,26,30]. It therefore seems that the stability of the bimetallic Au–Ag catalysts is independent of the nature of the support. The initial increase in activity within the first 2–3 h of reaction, which is not observed with monometallic gold, could be explained by restructuring of the particles and surface enrichment by one of the metals in the presence of the reactant mixture. For example, it has been shown in gold-based bimetallic systems such as Au–Ag [24], Au–Pd [52], and Au–Pt [53] that the surface composition and the particle structure change greatly with temperature. CO oxidation is a highly exothermic reaction, which could induce an increase in temperature in the particles and particle restructuring. It must also be noted that the catalytic activity of our Au–Ag/TiO_2 catalysts measured at 30 °C (Table 4) is very close than those of Au–Ag/MCM41 and Au–Ag/SiO_2 catalysts for similar reaction temperatures and particle sizes [30]. In contrast to the case of CO oxidation over monometallic gold catalysts, use of a reducible support such as titania does not lead to Au–Ag catalysts much more active than those supported on nonreducible supports such as silicas. This is a good indication that in the case of the Au–Ag catalysts, the reaction takes place on the metal particles, and that because oxygen can be activated on silver surface atoms, the involvement of the support in the reaction mechanism is either null or negligible. This would require confirmation with a comparative study involving Au–Ag catalysts prepared with the same method of preparation, containing the same particle size, and tested under strictly the same conditions.

5. Conclusions

We have developed a new method of preparation of Au–Ag/TiO_2 catalysts based on sequential deposition–precipitation of silver and then gold, which leads to rather small metal particles (~4 nm). Au–Ag/TiO_2 catalysts activated in H_2 at high temperature (550 °C) exhibit significantly higher activity in CO oxidation at RT and better temporal stability than monometallic gold catalysts containing particles of the same size (4 nm); monometallic silver catalyst is inactive at RT. These results confirm that there is a synergetic effect between gold and silver. In addition, the catalytic activities determined with the Au–Ag/TiO_2 catalysts compared well with those obtained for Au–Ag on nonreducible supports, indicating that the support is not involved in the reaction as in the case of monometallic gold catalysts and that molecular oxygen can be activated on silver atoms. On the other hand, the results obtained on the reducibility of the metal precursors in the dried samples, the metal particle size, and catalytic activity all give indirect evidence for interaction between Au and Ag in the reduced Au–Ag/TiO_2 samples, which was confirmed by micro-EDS analysis performed on individual particles. Moreover, as the temperature of activation under H_2 increases, the Au/Ag atomic ratio measured in the particles becomes closer to the value given by catalytic chemical analysis, indicating the formation of better-alloyed particles as the reduction temperature increases.

Acknowledgments

The authors acknowledge the scientific committee of synchrotron SOLEIL for giving them access to the SAMBA beamline, and the SOLEIL staff for efficient assistance, especially to Stephanie Belin. The authors also acknowledge CONACYT and CNRS for funding the collaboration between Mexico and France within the framework of an international bilateral program. We also thank the projects CONACYT 55154, Mexico and PAPIIT 108310, UNAM, Mexico for financial support.

References

[1] G.C. Bond, Catal. Today 72 (2002) 5.
[2] F. Moreau, G.C. Bond, Catal. Today 122 (2007) 215.
[3] G.C. Bond, C. Louis, D.T. Thompson, Catalysis by Gold, first ed., vol. 6, Imperial College Press, London, 2006.
[4] B. Roldan-Cuenya, Thin Solid Films 518 (2010) 3127.
[5] M. Haruta, T. Kobayashi, H. Sano, N. Yamada, Chem. Lett. 2 (1987) 405.
[6] J. Gong, C.B. Mullins, Acc. Chem. Res. 42 (2009) 1063.
[7] G.C. Bond, D.T. Thompson, Catal. Rev. Sci. Eng. 41 (1999) 319.
[8] X. Bokhimi, R. Zanella, A. Morales, J. Phys Chem. C 111 (2007) 15210.
[9] M. Haruta, Chem. Record 3 (2003) 75.
[10] R. Zanella, S. Giorgio, C.H. Shin, C.R. Henry, C. Louis, J. Catal. 222 (2004) 357.
[11] P. Konova, A. Naydenov, C. Venkov, D. Mehandjiev, D. Andreeva, T. Tabakova, J. Mol. Catal. A 213 (2004) 235.
[12] D. Andreeva, Gold Bull. 35 (2002) 82.
[13] F. Yang, M.S. Chen, D.W. Goodman, J. Phys. Chem. C 113 (2009) 254.
[14] D.E. Starr, S.K. Shaikhutdinov, H.J. Freund, Top. Catal. 36 (2005) 33.
[15] M.C. Raphulu, J. McPherson, E. van-der-Lingen, J.A. Anderson, M.S. Scurrell, Gold Bull. 43 (2010) 334.
[16] Y. Hao, M. Milhaylov, E. Ivanova, K. Hadjivanov, H. Knözinger, B.C. Gates, J. Catal. 261 (2009) 137.
[17] http://www.premchemltd.com/runtime/uploads/Files/Premier_Chemicals_NanAucat_Gold_Catalyst_Brochure.pdf.
[18] L. Guczi, G. Lu, Z. Zsoldos, Catal. Today 17 (1993) 459.
[19] H. Nakatsuji, Z.M. Hu, H. Nakai, Surf. Sci. 387 (1997) 328.
[20] A.L. de Oliveira, A. Wolf, F. Schüth, Catal. Lett. 73 (2001) 157.
[21] D. Tian, G. Yong, Y. Dai, X. Yan, S. Liu, Catal. Lett. 130 (2009) 211.
[22] Y. Iizuka, T. Miyamae, T. Miura, M. Okumura, M. Daté, M. Haruta, J. Catal. 262 (2009) 280.
[23] Y. Iizuka, A. Kawamoto, K. Akita, M. Daté, S. Tsubota, M. Haruta, Catal. Lett. 97 (2004) 203.
[24] A. Wang, C. Chang, C. Mou, J. Phys. Chem. B 109 (2005) 18860.
[25] A. Wang, Y.P. Hsieh, Y.F. Chen, C.Y. Mou, J. Catal. 237 (2006) 197.
[26] A.Q. Wang, J.H. Liu, S.D. Lin, T.S. Lin, C.Y. Mou, J. Catal. 233 (2005) 186.
[27] M. Hansen, Constitution of Binary Alloys, Mc Graw-Hill, New York, 1958.
[28] P.P. Elliott, Constitution of Binary Alloys, First Supplement, New York, 1965.
[29] F.A. Shunk, Constitution of Binary Alloys, Second Supplement, New York, 1969.
[30] X. Liu, A. Wang, X. Yang, T. Zhang, C.Y. Mou, D.S. Su, J. Li, Chem. Mater. 21 (2009) 410.
[31] C.-W. Yen, M.L. Lin, A. Wang, S.A. Chen, J.M. Chen, C.Y. Mou, J. Phys. Chem. C 113 (2009) 17831.
[32] A.R. Vilchis-Nestor, M. Avalos-Borja, S.A. Gómez, J.A. Hernández, A. Olivas, T.A. Zepeda, Appl. Catal. B 90 (2009) 64.
[33] R. Zanella, S. Giorgio, C.R. Henry, C. Louis, J. Phys. Chem. B 106 (2002) 7634.
[34] M. Haruta, Catal. Today 36 (1997) 153.
[35] X. Bokhimi, R. Zanella, C. Angeles, J. Phys. Chem. C 114 (2010) 14101.
[36] A. Gómez-Cortés, G. Díaz, R. Zanella, H. Ramírez, P. Santiago, J.M. Saniger, J. Phys. Chem. C 113 (2009) 9710.
[37] A. Hugon, L. Delannoy, J.-M. Krafft, C. Louis, 2010.
[38] R. Zanella, L. Delannoy, C. Louis, Appl. Catal. A 291 (2005) 62.
[39] R. Zanella, C. Louis, Catal. Today 107–08 (2005) 768.
[40] X. Sécordel, E. Berrier, M. Clément, Harrick Scientific Application Note 701204.
[41] A.L. Ankudinov, B. Ravel, J.J. Rehr, S.D. Conradson, Phys. Rev. B 58 (1998) 7565–7576.
[42] J.J. Kas, J. Vinson, N. Trcera, D. Cabaret, E.L. Shirley, J.J. Rehr, J. Phys. Conf. Ser. 190 (2009) 012009.
[43] http://home.kpn.nl/vanadovv/RedPot.html#ag.
[44] D. Andreeva, T. Tabakova, L. Ilieva, A. Naydenov, D. Mehanjiev, M.V. Abrashev, Appl. Catal. A 209 (2001) 291.
[45] V. Idakiev, L. Ilieva, D. Andreeva, J.L. Blin, L. Gigot, B.L. Su, Appl. Catal. A 243 (2003) 25.

[46] A. Sandoval, A. Gómez-Cortés, R. Zanella, G. Díaz, J.M. Saniger, J. Mol. Catal. A 278 (2007) 200.
[47] A. Hugon, L. Delannoy, C. Louis, Gold Bull. 41 (2008) 127.
[48] J.A. Reyes-Esqueda, A. Bautista-Salvador, R. Zanella, J. Nanosci. Nanotechnol. 8 (2008) 3843.
[49] D.I. Kondarides, X.E. Verykios, J. Catal. 158 (1996) 363.
[50] T.V.W. Janssens, A. Carlsson, A. Puig-Molina, B.S. Clausen, J. Catal. 240 (2006) 108.
[51] C. Wang, H. Yin, R. Chan, S. Peng, S. Dai, S. Sun, Chem. Mater. 21 (2009) 433.
[52] H.B. Liu, U. Pal, R. Perez, J.A. Ascencio, J. Phys. Chem. B 110 (2006) 5191.
[53] H.B. Liu, U. Pal, J.A. Ascencio, J. Phys. Chem. C 112 (2008) 19173.